NANO LETTERS

pubs.acs.org/NanoLett Letter

Pull-to-Peel of Two-Dimensional Materials for the Simultaneous Determination of Elasticity and Adhesion

Zheng Fang, Zhaohe Dai,* Bingjie Wang, Zhongzheng Tian, Chuanli Yu, Qing Chen, and Xianlong Wei*

Cite This: https://doi.org/10.1021/acs.nanolett.2c03145 Read Online

ACCESS | Metrics & More | Article Recommendations | Supporting Information

ABSTRACT: The flexible and clinging nature of ultrathin films requires an understanding of their elastic and adhesive properties in a wide range of circumstances from fabrications to applications. Simultaneously measuring both properties, however, is extremely difficult as the film thickness diminishes to the nanoscale. Here we address such difficulties through peeling by pulling thin films off from the substrates (we thus refer to it as "pull-to-peel"). Particularly, we perform *in situ* pull-to-peel of graphene and MoS_2 films in a scanning electron microscope and achieve simultaneous determination of their Young's moduli and adhesions to gold substrates. This is in striking contrast to other conceptually similar tests available in the literature, including indentation tests (only measuring elasticity) and spontaneous blisters (only measuring adhesion). Furthermore, we show a weakly nonlinear Hooke's relation for the pull-to-peel response of two-dimensional materials, which may be harnessed for the design of nanoscale force sensors or exploited in other thin-film systems.

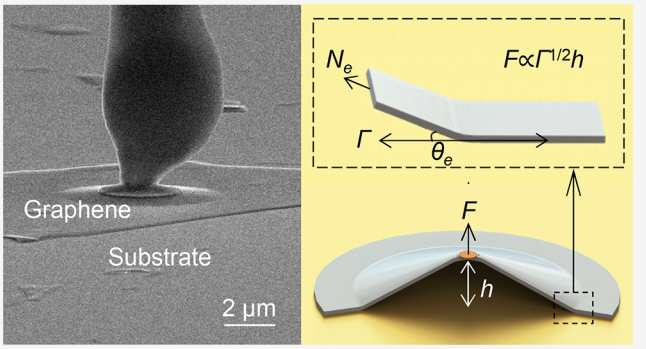

KEYWORDS: *2D materials, adhesion, elastic modulus, in situ SEM, blister test*

Thin films become increasingly flexible and willing to stick to other objects as their thickness decreases.[1,2] This fact makes the elasticity and adhesion of two-dimensional (2D) materials of interest from the point of view of fundamental mechanics, since they represent a class of thin films that could achieve atomic-level thickness.[3−8] In addition, knowing the elastic and adhesive properties of 2D materials is important in practice, particularly for the control, manipulation, and assembly of 2D materials into complex devices in which their extraordinary electronic and optical properties may be utilized.[9−14]

To understand the elastic and adhesive properties of a thin film, one may naturally pull and peel the material off a substrate so that the film is stretched and the film−substrate interface is delaminated.[15−19] However, such a direct methodology becomes extremely challenging as the thickness of the film diminishes to the nanoscale. The main challenges lie in the implementation and characterization of vertical loads, deflections, and interfacial delamination altogether at small scales. Herein, we address the challenges in pulling and peeling 2D materials for the elasticity and adhesion metrology with the aid of an *in situ* scanning electron microscope (SEM) (we thus term it "pull-to-peel" or "PTP").

We demonstrate the pull-to-peel method by focusing on graphene and MoS_2 nanoflakes on gold substrates. In particular, we perform pull-to-peel tests and develop relevant theories to interpret experimental data in terms of Young's moduli and adhesions, which show excellent agreement with previous experiments on graphene and MoS_2. PTP tests thus combine the key advantages of widely used nanomechanics techniques such as nanoindentation tests[20−25] and drum resonance tests[26−28] (only measure elasticity) and spontaneous blister tests (only measure adhesion),[29−35] reminiscent of the constant-molecule bulge test[36−39] (see more detailed comparison in Table S1 in the Supporting Information). In addition, we reveal a weakly nonlinear Hooke's law for the mechanical response of pull-to-peel, which could be useful not only for the design of nanoscale force sensors based on 2D materials but also for the elasticity and adhesion measurements of thin films at small scales beyond 2D materials.

In this work, we choose graphene and MoS_2 as typical metallic and semiconducting 2D materials and probe their elastic properties and adhesive properties via pull-to-peel tests. The samples for our PTP tests consist of multilayer 2D material nanoflakes transferred on an Au/Ti/SiO_2/Si substrate

Received: August 8, 2022
Revised: November 29, 2022

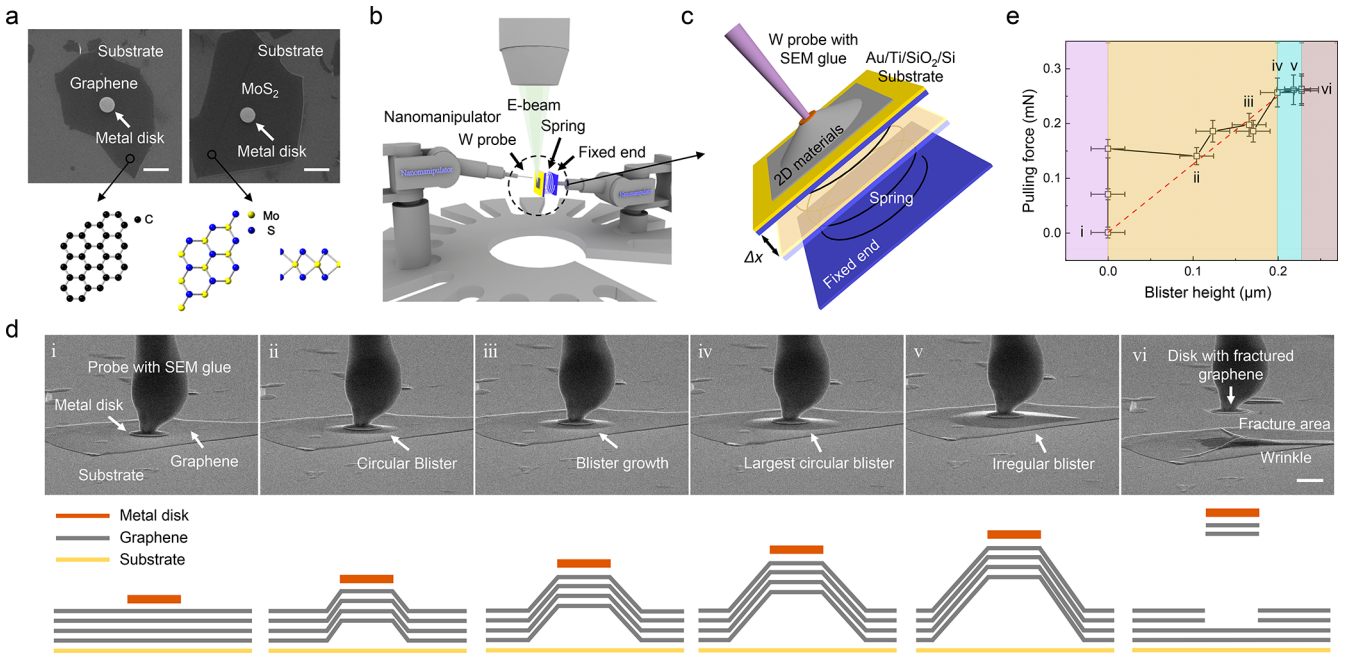

Figure 1. Experimental setup and results of *in situ* pull-to-peel tests. (a) Top-view SEM images (top panel) of a graphene sample (left) and an MoS_2 sample (right) for the PTP test and lattice structure schematic (bottom panel) of graphene and MoS_2. The sample consists of a multilayer 2D material nanoflake mechanically transferred on an Au/Ti/SiO_2/Si substrate and a metal disk deposited at the center of the nanoflake. Scale bar: 5 μm. (b, c) Schematics of the experimental setup for the *in situ* PTP test and the pulling force measurement. The W probe with SEM glue on its tip is controlled by a nanomanipulator to first approach/adhere to the metal disk and then retract/peel the 2D material nanoflake off from its substrate, where the substrate is connected to a spring and the pulling force can be measured based on the substrate displacement. (d) SEM images (top panel) and side-view schematics (bottom panel) of the PTP test on a graphene sample. Scale bar: 2 μm. (e) Measured pulling force as a function of the height of the produced blister for the sample shown in (d). Labels i–vi correspond to the frames of SEM images in (d) and the red dashed line is used to imply a linear force-height relation (which will be discussed in Figure 4c).

(unless otherwise stated) and a metal disk intentionally deposited at the center of each nanoflake through microfabrication (Figure 1a; see preparation details in Experimental Method in the Supporting Information). The nanoflakes are ~1–195 nm in thickness and 10–40 μm in lateral size, while the radius of the metal disks is fixed at around 1.5 μm (see more detailed summaries in Table S2 in the Supporting Information). Graphene and MoS_2 nanoflakes exhibit good hexagonal crystal structures, as shown by high-resolution transmission electron microscopy (TEM) in Figure S1.

We carry out the PTP test inside the SEM chamber with two nanomanipulators employed as a sample holder and a W probe controller, respectively (Figure 1b). Under the SEM observation, we are able to first push the W probe to make contact with and fixed to the metal disk (that has been deposited on the tested sample) and then gently pull the W probe back. As illustrated in Figure 1c,d, the 2D material sheet can be successfully pulled and peeled away from the substrate so that both elastic deformation and interfacial delamination take place. We note that the delamination occurs at the 2D material–Au interface rather than the 2D material–2D material interface because the conformability of the former is not as good as that of the latter (which is atomically smooth).[36] This can also be confirmed by a particular test and Raman spectroscopy in Figure S2, where a MoS_2 nanoflake was peeled off the substrate as a whole.

A particular feature of our proposed PTP tests is the experimentally measurable pulling force applied to the nanoflakes (distinct from spontaneous blister experiments in refs 29–35, 40, and 41). To achieve this, we connect the substrate with the samples to be tested to an elastic spring with spring stiffness k (Figure 1c). In each test k values ranging from 0.02 to 0.2 mN/μm are calibrated (see Figure S3). The pulling force F can thus be obtained simply by measuring the substrate displacement Δx (labeled in Figure 1c) through SEM observation and using $F = k\Delta x$.

We record the entire pull-to-peel process of the tested samples (see Supporting Video 1) and present a series of representative SEM images for a graphene nanoflake in Figure 1d. Frame i presents the initial contact state. The probe with SEM glue on its tip is controlled to approach and adhere to the metal disk deposited on graphene. Afterward, the probe is pulled back while the probe–metal disk contact remains due to the strong adhesion introduced by the SEM glue. Frame ii presents the moment at which a circular blister occurs. The subsequent frames iii and iv show the growth of this blister with increasing pulling displacements and delamination areas. During this process, we can simultaneously measure the pulling force (as shown in Figure 1e), the blister height, and the blister radius (defining the circular delamination area), distinguishing the pull-to-peel test presented here from previously reported indentation tests (that only measure force and loading displacement) and spontaneous blisters (that only measure delamination area and the profile of nanoflakes).

Before a complete PTP ends, we could also observe the generation of an irregular blister at the late stages shown in frame v in Figure 1d in some samples when the blister "feels" the outer physical boundary and sequentially the fracture of some outer layers of nanoflakes around the metal disk, as shown in frame vi. In PTP tests of MoS_2 samples, the mechanical behavior of the nanoflakes is rather similar (see Figure S4), but it is less likely to show irregular blisters.

https://doi.org/10.1021/acs.nanolett.2c03145
Nano Lett. XXXX, XXX, XXX–XXX

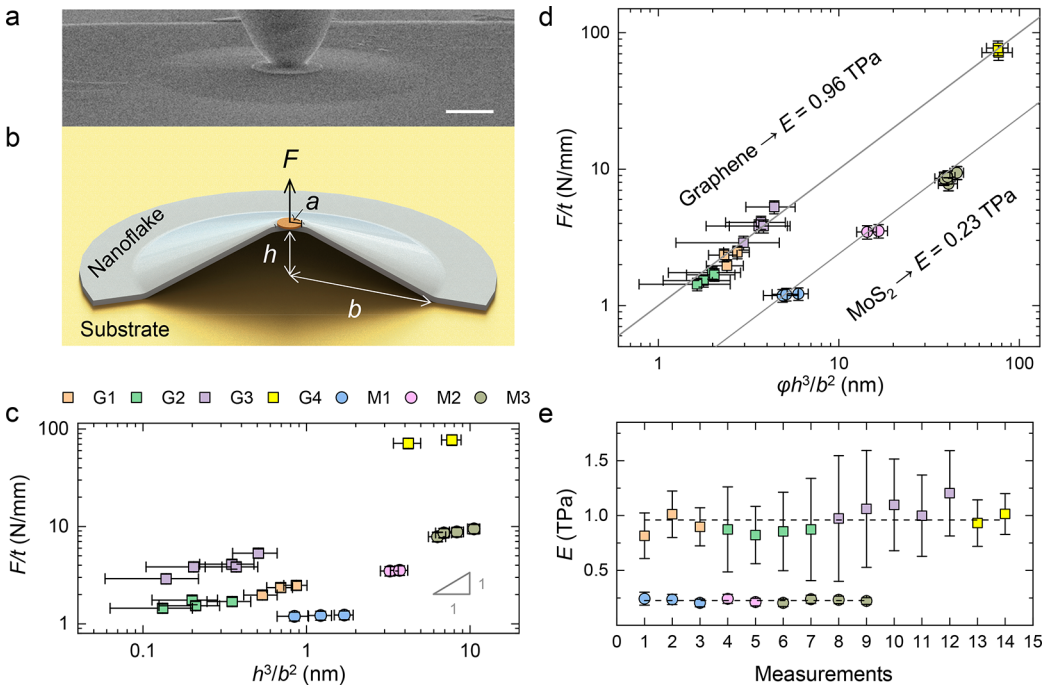

Figure 2. Geometry of relatively circular 2D material blisters and measurement of their elastic moduli. (a) SEM image of a circular graphene blister. Scale bar: 2 μm. (b) Schematic and notations for the analysis of a circular blister. The key parameters include the radius of the metal disk a, the pulling force F, the pulled blister height h, and the radius of the delamination area caused by the peeling of the nanoflake b. (c) F/t versus h^3/b^2 for four graphene samples (i.e., G1−G4) and three MoS_2 samples (i.e., M1−M3). (d) F/t versus $\varphi(a/b)h^3/b^2$ for these graphene and MoS_2 samples. The solid lines present the linear fitting with Young's moduli of 0.96 and 0.23 TPa for graphene and MoS_2, respectively. (e) Young's moduli obtained by plugging each set of (F,h,b) measured for graphene and MoS_2 samples into eq 3. Dashed lines present the average value, suggesting 0.96 ± 0.11 and 0.23 ± 0.01 TPa for graphene and MoS_2, respectively.

However, data obtained from such complex scenarios are typically difficult to interpret. This work therefore mainly focuses on the data measured from "regular" blisters, i.e., those seen in Figure 1d-ii−d-iv, particularly on how they are related to elastic and adhesive properties of the tested 2D materials.

It is natural to wonder whether the bending effect of the nanoflake is important in these blisters. We then consider a simple scaling argument. The curvature κ and the in-plane strain ε scale as h/b^2 and h^2/b^2, respectively, according to the elementary geometry in Figure 2a,b, where h and b are the height and radius of the blister, respectively. For a nanoflake of thickness t, bending stiffness B, and Young's modulus E, both the stretching energy of $\sim E\varepsilon^2 \times tb^2$ and bending energy of $\sim B\kappa^2 \times b^2$ are stored in the blister. However, comparing the two energies leads to the important parameter $\mathcal{K}_h = Eth^2/B$ (also called the Föppl−von Kármán number),[40,42] suggesting that the bending energy is important only when $\mathcal{K}_h$ is not much greater than unity. Since the bending stiffness of 2D materials is usually smaller than $Et^3/12(1-\nu^2)$ due to interlayer slips where ν is the Poisson's ratio,[43,44] we have $\mathcal{K}_h \gtrsim 12h^2/t^2$, i.e., $\mathcal{K}_h \gg 1$, in our experiments (Table S2)—stretching energy indeed dominates over bending energy in these blisters.

The large Föppl−von Kármán number in our blister systems allows for the interpretation of the measured data via a membrane-type analysis. One of the best-known examples of this type of analysis is the indentation of suspended thin membranes with edges clamped on a substrate. A key conclusion of this example is the nonlinear force−displacement relation that can be used for the measurement of Young's modulus

$$F = \alpha(\nu)\frac{Eth^3}{b^2} \tag{1}$$

where the prefactor $\alpha(\nu) = 0.867 + 0.2773\nu + 0.8052\nu^2$ was numerically determined (accurate within 0.7% for $0 < \nu < 0.5$).[45,46] We thus plot the measured F/t as a function of h^3/b^2 in Figure 2c and naively expect a linear relation with the slope that approximately indicates Young's moduli of nanoflakes. However, we find that (i) the data for graphene samples is quite nonlinear and (ii) graphene and MoS_2 samples show apparent stiffnesses of ∼10 and ∼1 TPa, respectively, which are significantly greater than those in previous reports (i.e., 1 TPa for graphene and 0.27 TPa for MoS_2).[20−22,47] Such inconsistency suggests a nontrivial role of the finite radius of the flat region on the top of the blister a (Figure 2a,b), considering that a/b ranges from 0.2 to 0.5 in our experiments (Table S2).

We then address the effect of the radius of the flat top region of the blister both numerically and analytically. The basic idea of numerical analysis is to apply the variational principle to the total free energy of the system

$$\Pi = U_{\text{elastic}} + U_{\text{external}} - \Gamma A_{\text{detach}} \tag{2}$$

where U_{elastic} is the stretching energy of the nanoflake, U_{external} is external work done by the probe (which vanishes in a displacement-controlled analysis), Γ can be thought of as the apparent adhesion energy per unit area of the 2D material−substrate interface, and $A_{\text{detach}} = \pi b^2$ is the detached interfacial area. A variational analysis $\delta\Pi = 0$ with $\delta b \neq 0$ can give the governing equations for the blister system; Also given are appropriate boundary conditions for solving such equations

https://doi.org/10.1021/acs.nanolett.2c03145
Nano Lett. XXXX, XXX, XXX−XXX

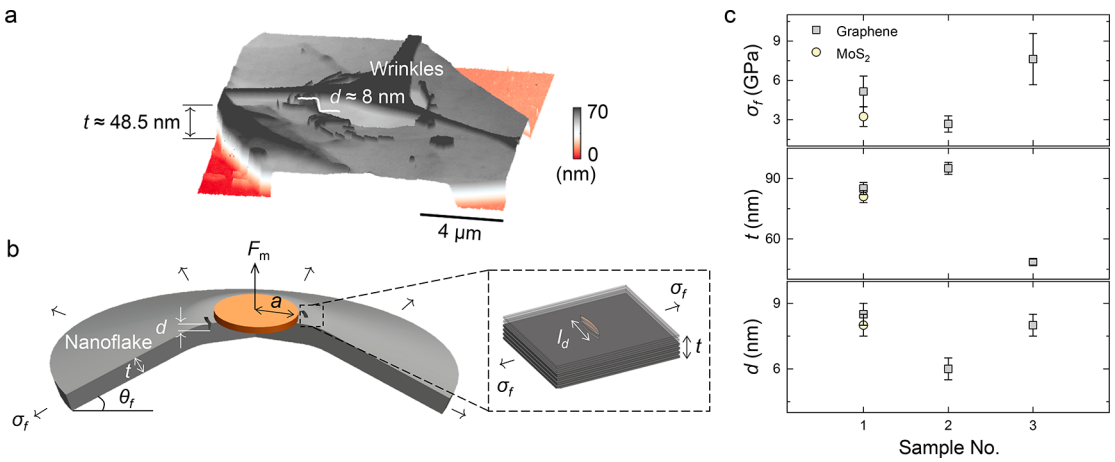

Figure 3. Fracture properties of 2D materials. (a) AFM image of a partially fractured graphene nanoflake after the PTP test, showing that ~8 nm thick graphene is peeled off from the parent graphene that is ~48.5 nm thick. Scale bar: 4 μm. (b) Schematic of the fracture region, where d, t, and σ_f are the thickness of the fractured 2D material, the thickness of the parent material, and the largest in-plane stress accumulated (ultimate strength) during the test, respectively. We use the inset to illustrate that the process of depositing a metal disk may introduce some defects into 2D material nanoflakes of length l_d. (c) σ_f and measured t and d for three graphene samples and one MoS_2 sample. Note that the data for the exceptional sample (trilayer graphene) is not shown here due to its dramatic differences in thickness.

and the unknown the blister radius b (see Section III in the Supporting Information).

Though we mainly solve this boundary value problem numerically for different Poisson's ratios in Section III in the Supporting Information, we also provide an approximate expression in a form similar to that for the indentation problem

$$F = \varphi(\nu; \zeta)Eth^3/b^2 \tag{3}$$

where $\zeta = a/b$ and

$$\varphi(\nu; \zeta) = \alpha(\nu)(1 - \zeta^{2/3})^{-3} \tag{4}$$

This simple expression combines Schwerin's solution for a specific Poisson's ratio (see more details in refs 45 and 48 and the numerical solution to the point-loaded indentation problem in eq 1). We numerically verified the applicability of eq 3 and calculated the detailed dependence of the prefactor φ on a/b for various Poisson's ratios (Figure S7). For both graphene (ν = 0.165) and MoS_2 (ν = 0.27), we find excellent agreement between numerics and eq 4. Besides, for all $0.1 < \nu < 0.5$, the error of eq 4 is within only 4%. In contrast, the errors produced by previously reported approximate solutions for blisters with a top flat end are up to at least 23% (Figure S7).[17,45,49]

An important implication of eq 4 is that the finite $\zeta = a/b$ of graphene and MoS_2 blisters in our experiments could change the prefactor by 1 order of magnitude (Figure S7). We, therefore, plot F/t as a function of $\varphi h^3/b^2$ in Figure 2d. As a result, excellent collapses of experimental data on linear curves are found, whose slopes (i.e., corresponding Young's moduli) are fitted to be 0.96 and 0.23 TPa for graphene (square markers) and MoS_2 (circular markers), respectively. These results agree very well with previously measured results using alternative methods, including bulge tests and indentation tests.[20−22,37,50] Such collapse and agreement may validate our proposed PTP tests and also justify our assumption of negligible residual stress in the theoretical model. Finally, in Figure 2e each set of measured data in Table S2 is plugged into eq 3 and hence exploited to extract Young's moduli of tested 2D materials—they are found to be 0.96 ± 0.11 and 0.23 ± 0.01 TPa for graphene and MoS_2, respectively.

We then briefly discuss the late stage of the PTP test during which the fracture phenomena may happen (Figure 1d-vi). Atomic force microscopy (AFM) images of the tested samples show that only part of the layers of the nanoflakes (about 6−9 nm in depth) is fractured and eventually peeled away by the metal disk (see an example in Figure 3a and the summary in Figure 3c). Our prime interest is the ultimate pulling force F_m, blister height h_m, and blister radius b_m that could be measured before the fracture of 2D materials (see all measured data in Table S2). We note that in this scenario the axisymmetry of blisters usually has broken; thus, b_m here is an average of the longest and shortest blister radii. Besides, the asymmetry renders any analytical progress elusive—we thus limit ourselves by discussing the fracture properties indicated by these ultimate parameters in a scaling sense.

For instance, based on the simple geometry and free body diagram in Figures 2b and 3b, respectively, we may estimate the ultimate in-plane stress caused by F_m for the tested nanoflake near the edge of the metal disk as

$$\sigma_f \approx \frac{F_m(b_m - a)}{2\pi a t h_m} \tag{5}$$

Plugging our data in Table S2 into eq 5 gives ultimate stresses of 5.2 ± 2 and 3.2 ± 0.6 GPa for graphene and MoS_2, respectively (Figure 3c). These values are on the order of $E/100$ and are much smaller than those from previous measurements on single-layer counterparts (which are close to the defect-free limit, i.e., $E/10$).[20−22] Note, however, that the fracture strength is found to be around 7 GPa in the bulge test of polymer-supported monolayer MoS_2.[51] We attribute such dramatic differences to the defects caused by the deposition of the metal disk to the nanoflakes, which needs to go through electron beam lithography and thermal evaporation coating processes (see discussion after Table S1). Alternatively, since the fracture toughness of graphene K_{Ic} has been well characterized in the literature,[52] we may use the concept of fracture mechanics for brittle materials, i.e.

https://doi.org/10.1021/acs.nanolett.2c03145
Nano Lett. XXXX, XXX, XXX−XXX

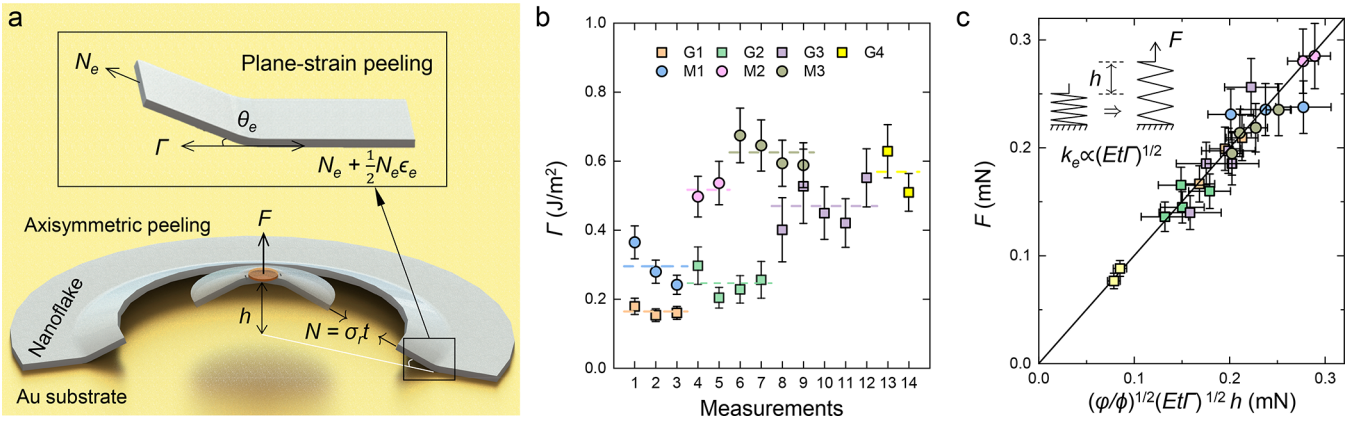

Figure 4. Adhesion between 2D materials and the underlying Au substrate. (a) Schematic illustration of the local force balances near the delamination front of the blister. Particularly, the inset invokes the concept of contact angle that is selected by the competition between elastic and adhesive forces. (b) Adhesion energy (per area) obtained for different 2D material samples by plugging our measurements into numerically verified eq 8. (c) Mechanical response of pull-and-peel of a nanoflake. By ruling out the weak nonlinearity of prefactors ϕ and φ that are explicitly given in eq 9, we obtain an excellent agreement between all measured data and a master line.

$$l_d \sim \frac{K_{Ic}^2}{\pi\sigma_f^2} \tag{6}$$

to gain some insights into typical lengths of defects in graphene nanoflakes introduced by e-beam irradiation and high temperature and high energy metal atoms bombardment (Figure 3b inset). Specifically, using $K_c \approx 4\ \mathrm{MPa}\sqrt{m}$ for graphene, we find l_d is on the order of 100 nm.[52] This small l_d (relative to the size of the metal disk) may justify that the influence of the defect on the measured elastic modulus and adhesion should be minimal. However, our PTP method is not positioned for the measurement of the ultimate strength of the nanoflakes unless the length of the defect is well-controlled and characterized.

We now discuss the adhesion Γ between the tested material and its substrate. The present *in situ* setup combines the key advantages of indentation experiments and spontaneous blister experiments, allowing the simultaneous measurements of applied pulling force and the delamination area that is peeled. Physically, such a peeled blister radius should be selected by the energetic competition between adhesion and elasticity. The mathematical presentation of this physical picture is to enforce a "no-pinning" condition (i.e., $\delta b \neq 0$; see Section III in the Supporting Information) when applying the variational analysis to eq 2,[53] giving rise to

$$N_e(1 - \cos\theta_e) - \Gamma + \frac{1}{2}N_e\varepsilon_e = 0 \tag{7}$$

where N_e, ε_e, and θ_e are radial stress, radial strain, and the rotation angle of the nanoflake evaluated at the edge of the blister, respectively (see Figure 4a). Notably, eq 7 is conceptually identical with Kendall's model for peeling a one-dimensional elastic ribbon off from a rigid substrate.[15]

To further make use of the aforementioned no-pinning condition for adhesion metrology, we approximate a cone shape for the blister to have $N_e = F/(2\pi b \sin\theta_e)$, $\theta_e \approx h/(b - a)$, and hence a simple expression for

$$\Gamma = \phi(\zeta)Fh/b^2 \tag{8}$$

where $\phi(\zeta) = \frac{1}{8\pi^2(1-\zeta)}[2\pi + (1-\nu^2)\varphi(\zeta)(1-\zeta)^3]$ and we used $\cos\theta_e \approx 1 - \theta_e^2/2$. In Section III in the Supporting Information, we compare eq 8 to numerical calculations and find the maximum error is within 4% for graphene and MoS_2 when $0.2 < \zeta < 0.5$. In contrast, the errors caused by other approximate models available in the literature, to the best of our knowledge, are at least 9% (see Figure S8).[17,49,54]

Since pulling forces, blister heights, and radii are all accessible in our PTP tests, we combine every set of measured data into eq 8 to extract adhesion energies for different samples (Figure 4b). It is found that, though the extracted values are relatively consistent for the same sample (indicated by the same color in Figure 4b), there are some variations from sample to sample even for the same material. Overall, however, the adhesion energies are distributed among 0.15−0.56 J/m^2 for graphene and 0.24−0.67 J/m^2 for MoS_2, agreeing with typical values suggested by previous measurements on relevant systems using other methods.[7,32] Note that G4 is adhesion of graphene to SiO_2, demonstrating that our method is not limited to a gold substrate. Also note that the scattering of adhesion in experiments might not be surprising, since adhesion is an interface property relying heavily on the quality of the material−substrate interfaces, which is extremely vulnerable to manufacturing and environmental conditions.[7,8,55,56]

Having shown the use of our proposed pull-to-peel tests for the measurements of elastic and adhesive properties of 2D materials, we conclude by discussing the mechanical response of pulling and peeling a nanoflake. In particular, combining eq 3 (used for Young's modulus measurements) and eq 8 (used for adhesion measurements) gives

$$F = (\varphi/\phi)^{1/2}(Et\Gamma)^{1/2}h \tag{9}$$

This immediately suggests Hooke's law for the pulling force−blister height relation (Figure 4c), while there is some weak nonlinearity due to the dependence of the prefactor on the blister size. Hooke's law for the pulling force−blister height relation agrees well with our approximately linear F−h relation in the experimental data of Figure 1e. Moreover, since both pulling and peeling take place, the apparent stiffness for such an F−h relation is equally contributed by in-plane stiffness of the nanoflake and adhesion between the nanoflake and the substrate—$\sqrt{Et\Gamma}$. Such behavior is intrinsically different from the F−h^3 relation in nanoindentation tests of suspended

https://doi.org/10.1021/acs.nanolett.2c03145
Nano Lett. XXXX, XXX, XXX−XXX

nanoflakes in which the edge of the nanoflakes is clamped (delamination is therefore suppressed).[20−22,24,25] In Figure 4c, we plot the pulling force as a function of the right-hand side term of eq 9 and find the agreement between our results and the spring model (solid line), where the specific thickness, Young's modulus, and adhesion take the measured values in the preceding section, i.e., Figures 3c (middle panel), 2e (dashed lines), and 4b (dashed lines), respectively. A direct implication of this collapse is that, in PTP experiments where the blister radii are not readily determined, the pulling stiffness could be exploited to determine the adhesion with in-plane stiffness of the nanoflake known, or the other way around.

In conclusion, this work has demonstrated our attempt to realize the classical blister test for nanometer-thick thin films. The existing challenges in applying controlled loads and measuring the deformations have been addressed by an *in situ* pull-to-peel approach. We have also provided analytical solutions with improved accuracy (compared to those in the literature) to account for the effect of the finite size of the loading zone so that the elastic and adhesive properties of the nanoflakes can be readily extracted. We have also uncovered a simple Hookean mechanism when pulling and peeling 2D materials nanoflakes—this might be harnessed to design novel force sensors in micro-/nanoelectromechanical systems.

■ ASSOCIATED CONTENT

Supporting Information

The Supporting Information is available free of charge at https://pubs.acs.org/doi/10.1021/acs.nanolett.2c03145.

Video of *in situ* pull-to-peel test on multilayer graphene (MP4)

Experimental methods, complementary experimental results including SEM images of 2D materials of different thicknesses and detailed raw data, and theoretical modeling details including a variational analysis and a comparison between our model and previous models (PDF)

■ AUTHOR INFORMATION

Corresponding Authors

Zhaohe Dai − *Department of Mechanics and Engineering Science, College of Engineering, Peking University, Beijing 100871, People's Republic of China;* orcid.org/0000-0002-5205-089X; Email: daizh@pku.edu.cn

Xianlong Wei − *Key Laboratory for the Physics and Chemistry of Nanodevices, School of Electronics, Peking University, Beijing 100871, People's Republic of China;* orcid.org/0000-0002-1181-9500; Email: weixl@pku.edu.cn

Authors

Zheng Fang − *Key Laboratory for the Physics and Chemistry of Nanodevices, School of Electronics, Peking University, Beijing 100871, People's Republic of China;* orcid.org/0000-0003-3304-5726

Bingjie Wang − *Key Laboratory for the Physics and Chemistry of Nanodevices, School of Electronics, Peking University, Beijing 100871, People's Republic of China*

Zhongzheng Tian − *School of Integrated Circuits, Peking University, Beijing 100871, People's Republic of China*

Chuanli Yu − *Department of Mechanics and Engineering Science, College of Engineering, Peking University, Beijing 100871, People's Republic of China*

Qing Chen − *Key Laboratory for the Physics and Chemistry of Nanodevices, School of Electronics, Peking University, Beijing 100871, People's Republic of China;* orcid.org/0000-0002-7919-5159

Complete contact information is available at: https://pubs.acs.org/10.1021/acs.nanolett.2c03145

Author Contributions

Z.F. and X.W. designed the experiments. Z.F. performed sample fabrication and PTP tests and analyzed experimental data. Z.D. proposed theoretical models and performed numerical analysis. Z.F., Z.D., and X.W. wrote the manuscript. Z.F. and Z.T. performed AFM experiments. B.W. and Q.C. contributed valuable discussions. X.W. supervised the project. All authors have read the manuscript and agree with its contents.

Notes

The authors declare no competing financial interest.

■ ACKNOWLEDGMENTS

This work was supported by the NSF of China (Grant Nos. 11874068, 11890671, and 62022007). We thank Luqi Liu, Mingchao Liu, and Yueguang Wei for many useful discussions. We thank Jiamin Tian for assisting with TEM characterization.

■ REFERENCES

(1) Style, R. W.; Jagota, A.; Hui, C.-Y.; Dufresne, E. R. Elastocapillarity: Surface Tension and the Mechanics of Soft Solids. *Annu. Rev. Condens. Matter Phys.* **2017**, *8* (1), 99−118.

(2) Bico, J.; Reyssat, E.; Roman, B. Elastocapillarity: When Surface Tension Deforms Elastic Solids. *Annu. Rev. Fluid Mech.* **2018**, *50* (1), 629−659.

(3) Novoselov, K. S.; Mishchenko, A.; Carvalho, A.; Castro Neto, A. H. 2D materials and van der Waals heterostructures. *Science* **2016**, *353* (6298), aac9439.

(4) Li, X.; Tao, L.; Chen, Z.; Fang, H.; Li, X.; Wang, X.; Xu, J.-B.; Zhu, H. Graphene and related two-dimensional materials: Structure-property relationships for electronics and optoelectronics. *Appl. Phys. Rev.* **2017**, *4* (2), 021306.

(5) Li, P.; Kang, Z.; Zhang, Z.; Liao, Q.; Rao, F.; Lu, Y.; Zhang, Y. In situ microscopy techniques for characterizing the mechanical properties and deformation behavior of two-dimensional (2D) materials. *Mater. Today* **2021**, *51*, 247−272.

(6) Akinwande, D.; Brennan, C. J.; Bunch, J. S.; Egberts, P.; Felts, J. R.; Gao, H.; Huang, R.; Kim, J.-S.; Li, T.; Li, Y.; Liechti, K. M.; Lu, N.; Park, H. S.; Reed, E. J.; Wang, P.; Yakobson, B. I.; Zhang, T.; Zhang, Y.-W.; Zhou, Y.; Zhu, Y. A review on mechanics and mechanical properties of 2D materials—Graphene and beyond. *Extreme Mech. Lett.* **2017**, *13*, 42−77.

(7) Dai, Z.; Lu, N.; Liechti, K. M.; Huang, R. Mechanics at the interfaces of 2D materials: Challenges and opportunities. *Curr. Opin. Solid State Mater. Sci.* **2020**, *24* (4), 100837.

(8) Liechti, K. M. Characterizing the Interfacial Behavior of 2D Materials: a Review. *Exp. Mech.* **2019**, *59* (3), 395−412.

(9) Dai, Z.; Liu, L.; Zhang, Z. Strain Engineering of 2D Materials: Issues and Opportunities at the Interface. *Adv. Mater.* **2019**, *31* (45), 1805417.

(10) Frisenda, R.; Navarro-Moratalla, E.; Gant, P.; De Lara, D. P.; Jarillo-Herrero, P.; Gorbachev, R. V.; Castellanos-Gomez, A. Recent progress in the assembly of nanodevices and van der Waals heterostructures by deterministic placement of 2D materials. *Chem. Soc. Rev.* **2018**, *47* (1), 53−68.

(11) Akinwande, D.; Petrone, N.; Hone, J. Two-dimensional flexible nanoelectronics. *Nat. Commun.* **2014**, *5* (1), 1−12.

(12) Zhan, H.; Guo, D.; Xie, G. Two-dimensional layered materials: from mechanical and coupling properties towards applications in electronics. *Nanoscale* **2019**, *11* (28), 13181−13212.
(13) Kim, S. J.; Choi, K.; Lee, B.; Kim, Y.; Hong, B. H. Materials for flexible, stretchable electronics: graphene and 2D materials. *Annu. Rev. Mater. Res.* **2015**, *45*, 63−84.
(14) Annett, J.; Cross, G. L. W. Self-assembly of graphene ribbons by spontaneous self-tearing and peeling from a substrate. *Nature* **2016**, *535* (7611), 271−275.
(15) Kendall, K. Thin-film peeling-the elastic term. *J. Phys. D: Appl. Phys.* **1975**, *8* (13), 1449.
(16) Chopin, J.; Vella, D.; Boudaoud, A. The liquid blister test. *Proc. Math. Phys. Eng. Sci.* **2008**, *464* (2099), 2887−2906.
(17) Afferrante, L.; Carbone, G.; Demelio, G.; Pugno, N. Adhesion of elastic thin films: double peeling of tapes versus axisymmetric peeling of membranes. *Tribol. Lett.* **2013**, *52* (3), 439−447.
(18) Miskin, M. Z.; Sun, C.; Cohen, I.; Dichtel, W. R.; McEuen, P. L. Measuring and manipulating the adhesion of graphene. *Nano Lett.* **2018**, *18* (1), 449−454.
(19) Xue, Z.; Chen, G.; Wang, C.; Huang, R. Peeling and sliding of graphene nanoribbons with periodic van der Waals interactions. *J. Mech. Phys. Solids* **2022**, *158*, 104698.
(20) Lee, C.; Wei, X.; Kysar, J. W.; Hone, J. Measurement of the elastic properties and intrinsic strength of monolayer graphene. *Science* **2008**, *321* (5887), 385−388.
(21) Bertolazzi, S.; Brivio, J.; Kis, A. Stretching and Breaking of Ultrathin MoS2. *ACS Nano* **2011**, *5* (12), 9703−9709.
(22) Castellanos-Gomez, A.; Poot, M.; Steele, G. A.; van der Zant, H. S. J.; Agraït, N.; Rubio-Bollinger, G. Elastic Properties of Freely Suspended MoS2 Nanosheets. *Adv. Mater.* **2012**, *24* (6), 772−775.
(23) Falin, A.; Cai, Q.; Santos, E. J. G.; Scullion, D.; Qian, D.; Zhang, R.; Yang, Z.; Huang, S.; Watanabe, K.; Taniguchi, T.; Barnett, M. R.; Chen, Y.; Ruoff, R. S.; Li, L. H. Mechanical properties of atomically thin boron nitride and the role of interlayer interactions. *Nat. Commun.* **2017**, *8* (1), 15815.
(24) Sun, Y.; Pan, J.; Zhang, Z.; Zhang, K.; Liang, J.; Wang, W.; Yuan, Z.; Hao, Y.; Wang, B.; Wang, J.; Wu, Y.; Zheng, J.; Jiao, L.; Zhou, S.; Liu, K.; Cheng, C.; Duan, W.; Xu, Y.; Yan, Q.; Liu, K. Elastic Properties and Fracture Behaviors of Biaxially Deformed, Polymorphic MoTe2. *Nano Lett.* **2019**, *19* (2), 761−769.
(25) Liu, K.; Yan, Q.; Chen, M.; Fan, W.; Sun, Y.; Suh, J.; Fu, D.; Lee, S.; Zhou, J.; Tongay, S.; Ji, J.; Neaton, J. B.; Wu, J. Elastic Properties of Chemical-Vapor-Deposited Monolayer MoS2, WS2, and Their Bilayer Heterostructures. *Nano Lett.* **2014**, *14* (9), 5097−5103.
(26) Lee, J.; Wang, Z.; He, K.; Shan, J.; Feng, P. X. L. High Frequency MoS2 Nanomechanical Resonators. *ACS Nano* **2013**, *7* (7), 6086−6091.
(27) Wang, Z.; Jia, H.; Zheng, X.-Q.; Yang, R.; Ye, G. J.; Chen, X. H.; Feng, P. X. L. Resolving and Tuning Mechanical Anisotropy in Black Phosphorus via Nanomechanical Multimode Resonance Spectromicroscopy. *Nano Lett.* **2016**, *16* (9), 5394−5400.
(28) Zheng, X.-Q.; Lee, J.; Feng, P. X. L. Hexagonal boron nitride nanomechanical resonators with spatially visualized motion. *Microsyst. Nanoeng.* **2017**, *3* (1), 17038.
(29) Zong, Z.; Chen, C.-L.; Dokmeci, M. R.; Wan, K.-t. Direct measurement of graphene adhesion on silicon surface by intercalation of nanoparticles. *J. Appl. Phys.* **2010**, *107* (2), 026104.
(30) Wang, J.; Sorescu, D. C.; Jeon, S.; Belianinov, A.; Kalinin, S. V.; Baddorf, A. P.; Maksymovych, P. Atomic intercalation to measure adhesion of graphene on graphite. *Nat. Commun.* **2016**, *7* (1), 13263.
(31) Sanchez, D. A.; Dai, Z.; Wang, P.; Cantu-Chavez, A.; Brennan, C. J.; Huang, R.; Lu, N. Mechanics of spontaneously formed nanoblisters trapped by transferred 2D crystals. *Proc. Natl. Acad. Sci. U.S.A.* **2018**, *115* (31), 7884−7889.
(32) Torres, J.; Zhu, Y.; Liu, P.; Lim, S. C.; Yun, M. Adhesion Energies of 2D Graphene and MoS2 to Silicon and Metal Substrates. *Phys. Status Solidi A* **2018**, *215* (1), 1700512.
(33) Blundo, E.; Yildirim, T.; Pettinari, G.; Polimeni, A. Experimental Adhesion Energy in van der Waals Crystals and Heterostructures from Atomically Thin Bubbles. *Phys. Rev. Lett.* **2021**, *127* (4), 046101.
(34) Lou, L.; Chen, P.; Xiang, C.; Peng, J.; Zhang, S. Measuring cohesive energy of van der Waals heterostructures by nanoparticle intercalation method. *Mech. Mater.* **2022**, *166*, 104243.
(35) Wang, W.; Ma, X.; Dai, Z.; Zhang, S.; Hou, Y.; Wang, G.; Li, Q.; Zhang, Z.; Wei, Y.; Liu, L. Mechanical Behavior of Blisters Spontaneously Formed by Multilayer 2D Materials. *Adv. Mater. Interfaces* **2022**, *9* (12), 2101939.
(36) Koenig, S. P.; Boddeti, N. G.; Dunn, M. L.; Bunch, J. S. Ultrastrong adhesion of graphene membranes. *Nat. Nanotechnol.* **2011**, *6* (9), 543−546.
(37) Lloyd, D.; Liu, X.; Boddeti, N.; Cantley, L.; Long, R.; Dunn, M. L.; Bunch, J. S. Adhesion, Stiffness, and Instability in Atomically Thin MoS2 Bubbles. *Nano Lett.* **2017**, *17* (9), 5329−5334.
(38) Wang, G.; Dai, Z.; Wang, Y.; Tan, P.; Liu, L.; Xu, Z.; Wei, Y.; Huang, R.; Zhang, Z. Measuring Interlayer Shear Stress in Bilayer Graphene. *Phys. Rev. Lett.* **2017**, *119* (3), 036101.
(39) Dai, Z.; Hou, Y.; Sanchez, D. A.; Wang, G.; Brennan, C. J.; Zhang, Z.; Liu, L.; Lu, N. Interface-Governed Deformation of Nanobubbles and Nanotents Formed by Two-Dimensional Materials. *Phys. Rev. Lett.* **2018**, *121* (26), 266101.
(40) Dai, Z.; Sanchez, D. A.; Brennan, C. J.; Lu, N. Radial buckle delamination around 2D material tents. *J. Mech. Phys. Solids* **2020**, *137*, 103843.
(41) Fang, Z.; Li, X.; Shi, W.; Li, Z.; Guo, Y.; Chen, Q.; Peng, L.; Wei, X. Interlayer Binding Energy of Hexagonal MoS2 as Determined by an In Situ Peeling-to-Fracture Method. *J. Phys. Chem. C* **2020**, *124* (42), 23419−23425.
(42) Dai, Z.; Lu, N. Poking and bulging of suspended thin sheets: Slippage, instabilities, and metrology. *J. Mech. Phys. Solids* **2021**, *149*, 104320.
(43) Han, E.; Yu, J.; Annevelink, E.; Son, J.; Kang, D. A.; Watanabe, K.; Taniguchi, T.; Ertekin, E.; Huang, P. Y.; van der Zande, A. M. Ultrasoft slip-mediated bending in few-layer graphene. *Nat. Mater.* **2020**, *19* (3), 305−309.
(44) Wang, G.; Dai, Z.; Xiao, J.; Feng, S.; Weng, C.; Liu, L.; Xu, Z.; Huang, R.; Zhang, Z. Bending of Multilayer van der Waals Materials. *Phys. Rev. Lett.* **2019**, *123* (11), 116101.
(45) Vella, D.; Davidovitch, B. Indentation metrology of clamped, ultra-thin elastic sheets. *Soft Matter* **2017**, *13* (11), 2264−2278.
(46) Komaragiri, U.; Begley, M.; Simmonds, J. The mechanical response of freestanding circular elastic films under point and pressure loads. *J. Appl. Mech.* **2005**, *72* (2), 203−212.
(47) Di Giorgio, C.; Blundo, E.; Pettinari, G.; Felici, M.; Lu, Y.; Cucolo, A. M.; Polimeni, A.; Bobba, F. Nanoscale Measurements of Elastic Properties and Hydrostatic Pressure in H2-Bulged MoS2-Membranes. *Adv. Mater. Interfaces* **2020**, *7* (23), 2001024.
(48) Schwerin, E. ber Spannungen und Form‰ nderungen kreisringfrmiger Membranen. *Z. Angew. Math Phys.* **1929**, *9* (6), 482−483.
(49) Wan, K.-T. Adherence of an axisymmetric flat punch on a thin flexible membrane. *J. Adhes* **2001**, *75* (4), 369−380.
(50) Di Giorgio, C.; Blundo, E.; Pettinari, G.; Felici, M.; Polimeni, A.; Bobba, F. Exceptional Elasticity of Microscale Constrained MoS2 Domes. *ACS Appl. Mater. Interfaces* **2021**, *13* (40), 48228−48238.
(51) Yang, R.; Lee, J.; Ghosh, S.; Tang, H.; Sankaran, R. M.; Zorman, C. A.; Feng, P. X. L. Tuning Optical Signatures of Single- and Few-Layer MoS2 by Blown-Bubble Bulge Straining up to Fracture. *Nano Lett.* **2017**, *17* (8), 4568−4575.
(52) Zhang, P.; Ma, L.; Fan, F.; Zeng, Z.; Peng, C.; Loya, P. E.; Liu, Z.; Gong, Y.; Zhang, J.; Zhang, X.; Ajayan, P. M.; Zhu, T.; Lou, J. Fracture toughness of graphene. *Nat. Commun.* **2014**, *5* (1), 3782.
(53) Dai, Z.; Rao, Y.; Lu, N. Two-dimensional crystals on adhesive substrates subjected to uniform transverse pressure. *Int. J. Solids Struct.* **2022**, *257*, 111829.
(54) Williams, J. Energy release rates for the peeling of flexible membranes and the analysis of blister tests. *Int. J. Fract.* **1997**, *87* (3), 265−288.

https://doi.org/10.1021/acs.nanolett.2c03145
Nano Lett. XXXX, XXX, XXX−XXX

(55) Megra, Y. T.; Suk, J. W. Adhesion properties of 2D materials. *J. Phys. D: Appl. Phys.* **2019**, *52* (36), 364002.
(56) Di Giorgio, C.; Blundo, E.; Pettinari, G.; Felici, M.; Bobba, F.; Polimeni, A. Mechanical, Elastic, and Adhesive Properties of Two-Dimensional Materials: From Straining Techniques to State-of-the-Art Local Probe Measurements. *Adv. Mater. Interfaces* **2022**, *9* (13), 2102220.

https://doi.org/10.1021/acs.nanolett.2c03145
Nano Lett. XXXX, XXX, XXX−XXX

Supporting Information

Pull-to-peel of two-dimensional materials for the simultaneous determination of elasticity and adhesion

Zheng Fang[1], Zhaohe Dai[2,*], Bingjie Wang[1], Zhongzheng Tian[3], Chuanli Yu[2], Qing Chen[1], Xianlong Wei[1,*]

[1]Key Laboratory for the Physics and Chemistry of Nanodevices, School of Electronics, Peking University, Beijing 100871, China
[2]Department of Mechanics and Engineering Science, College of Engineering, Peking University, Beijing 100871, China
[3]School of Integrated Circuits, Peking University, Beijing 100871, China

[*]Correspondence and requests for materials should be addressed to Z.D. (email: daizh@pku.edu.cn) and X.W. (email: weixl@pku.edu.cn)

In this Supporting Information (SI), we provide method in Section I, experimental results in Section II that are complementary to those in the main text and theoretical results in Section III that may support our claims in the main text about the accuracy of analytical models.

Section I: Experimental method

Sample preparation and characterization. Au/Ti film (~70/20 nm in thickness) is deposited on SiO_2/Si (~285 nm/500 μm in thickness) substrate by e-beam thermal evaporation deposition (Texas Instruments DE400). 2D material nanoflakes are then transferred on Au/Ti film by mechanical exfoliation method. Large-area and flat nanoflakes of 2D materials are selected for subsequent sample fabrication under an optical microscope (Carl Zeiss Axio Imager). Through standard electron beam lithography (Raith voyager), e-beam thermal evaporation deposition, and lift-off processes, circular Au/Ti disks (~70/20 nm in thickness) with radii of 1.5 μm are fabricated at the center of selected nanoflakes. The thickness of 2D material nanoflakes and the fractured groove (if any after PTP tests) are measured by AFM (Bruker dimension icon) in tapping mode.

Pull-to-peel tests. The PTP tests are performed in an SEM (FEI-Quanta 600F) equipped with two nanomanipulators (Kleindiek MM3A). One nanomanipulator is used to support the fixed end of a spring for the pulling force measurement. Another nanomanipulator is used to support and manipulate a W probe for pulling the nanoflakes of 2D materials. To perform a PTP test, a W probe with some SEM glue (Kleindiek SEMGLU) on its tip is firstly manipulated to contact the metal disk fabricated on a nanoflake of 2D materials, then the contact area between the W probe and the metal disk is irradiated by 20 kV SEM electron beam to solidify the SEM glue and strengthen the connection between W probe and metal disk so that the mechanical strength of the contact is strong enough for the subsequent peeling. To pull and peel a nanoflake of 2D materials off, the W probe gently retreats perpendicular to the substrate plane till the fracture of 2D materials.

Section II: Additional experimental details

1. TEM images of graphene and MoS_2

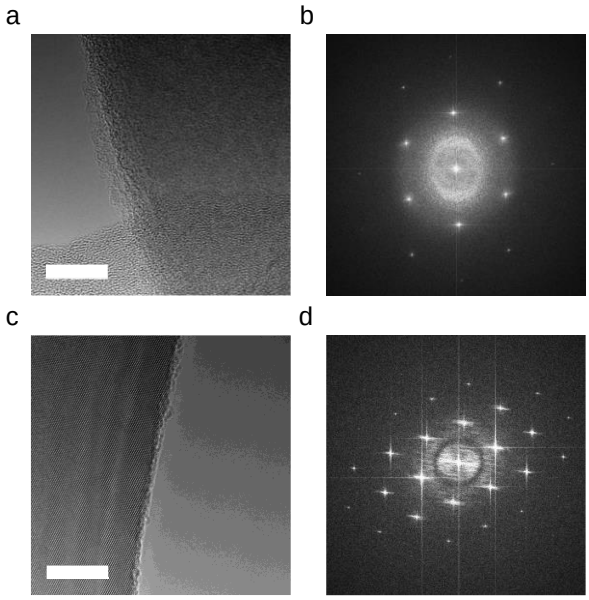

Fig. S1. TEM images of mechanically exfoliated graphene and MoS_2 nanoflake. **a.** High-resolution TEM image of a graphene nanoflake, scale bar: 10 nm. **b.** Fast Fourier transform pattern of the graphene image, showing a hexagonal crystalline structure. **c**. High-resolution TEM image of a MoS_2 nanoflake, scale bar: 10 nm. **d**. Fast Fourier transform pattern of the MoS_2 image, showing a hexagonal crystalline structure.

2. Peeling-off of the MoS_2 nanoflake as a whole

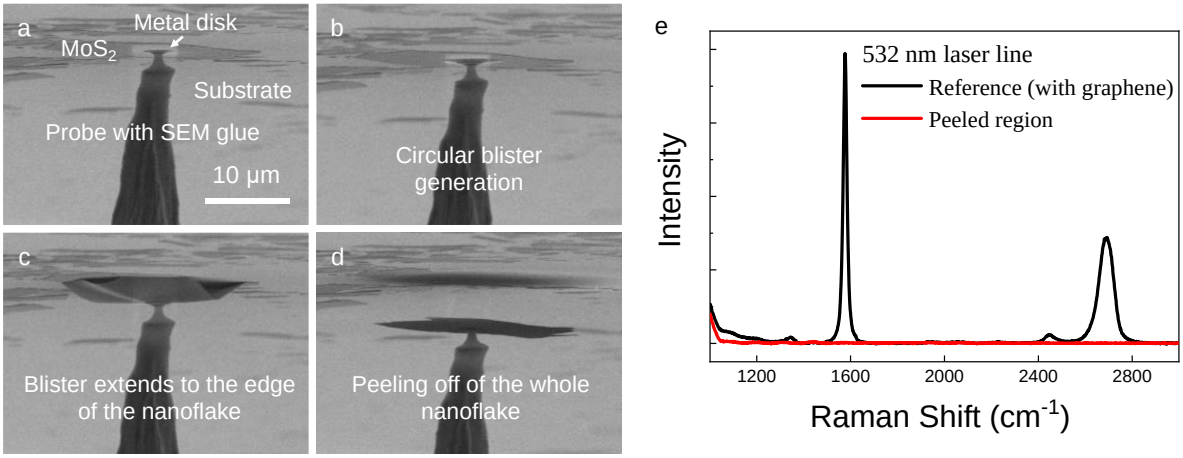

Fig. S2. ***In-situ*** **pull-to-peel test on MoS_2 in the case that the whole nanoflake can be peeled off. a-d.** SEM images. **e.** Raman spectrum.

3. Spring stiffness coefficient calibration

The tip of the force sensor (Handpi HP series digital force gauge) is fixed with the spring sample table that is placed on high precision vertical linear displacement stage and then controlled to pull. During the pulling process, the force-displacement curve is recorded to obtain the tensile spring stiffness.

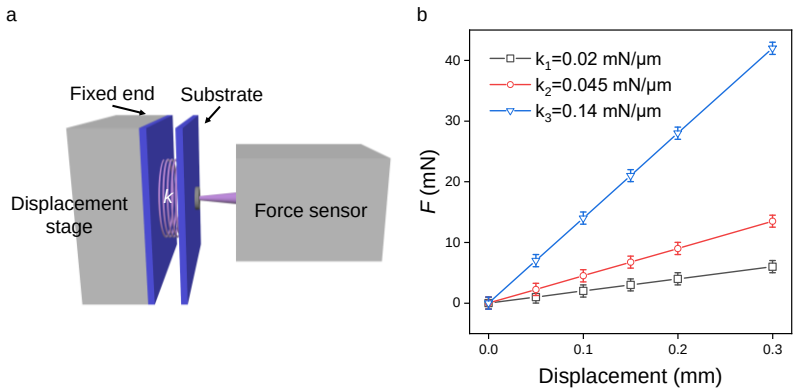

Fig. S3. a. Schematics of Spring stiffness coefficient calibration process. **b**. Typical spring stiffness curves of the elastic springs used in our experiments.

4. Pull-to-peel test on MoS_2 nanoflake

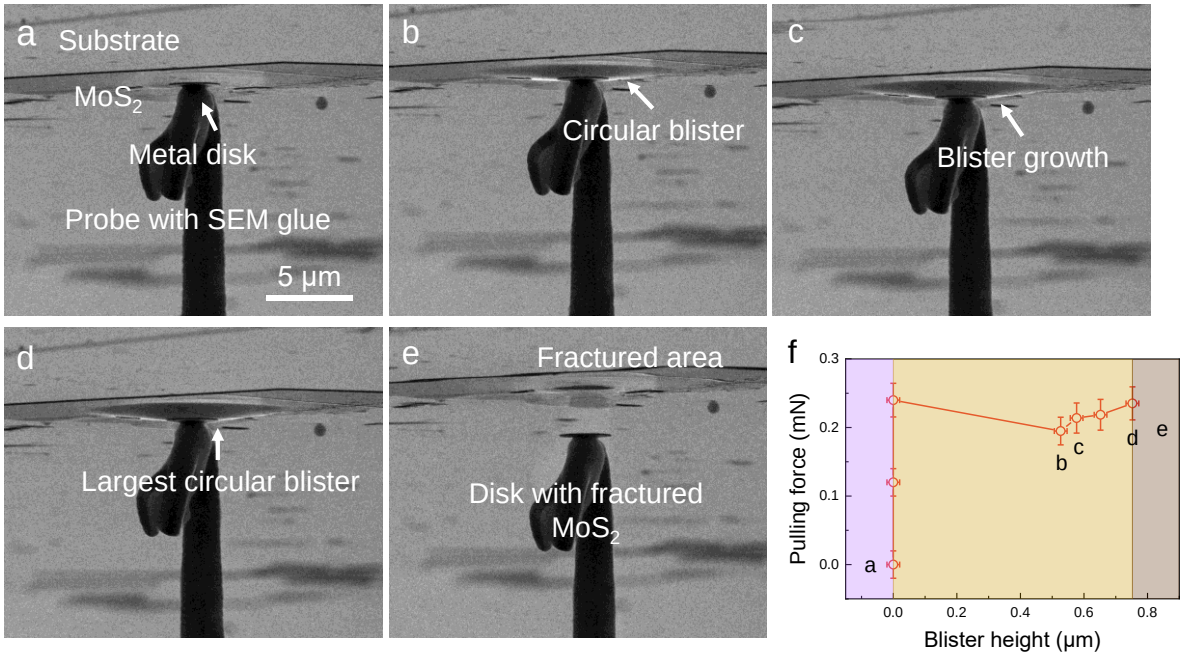

Fig. S4. SEM images of *in-situ* pull-to-peel test on MoS_2. a. Initial contact state: The probe with SEM glue on its tip is controlled to adhere to the metal disk on MoS_2. Scale bar: 5 μm. **b.** Circular blister generation: The circular blister of graphene generates when the probe is pulled perpendicular to the basal plane of MoS_2 to peel it up. **c**. The circular blister growth **d.** Largest

circular blister. **e.** Blister fracture: The graphene at the periphery of the metal disk fractures under the maximum pulling force. **f.** Measured pulling force as a function of blister height.

5. PTP test on trilayer graphene on SiO_2 substrate.

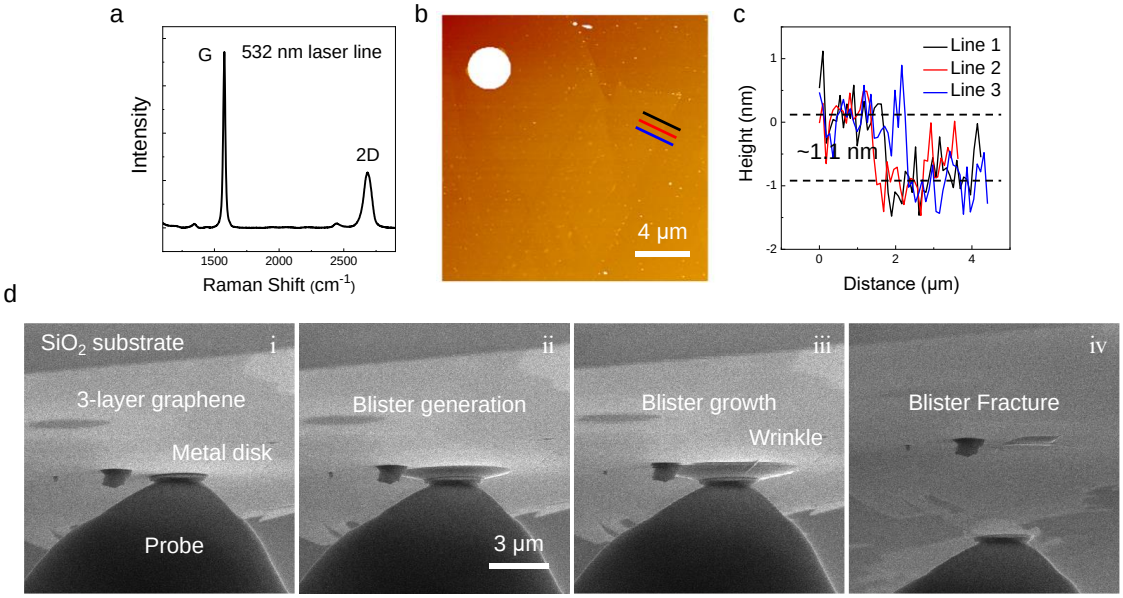

Fig. S5. PTP test on trilayer graphene on SiO_2 substrate. a. Raman spectrum of the graphene. **b.** AFM image. **c.** height profile along the lines in b. **d.** SEM images of the PTP test, where regular blister generation (i and ii), blister growth (iii), wrinkle generation and blister fracture (iv) are observed.

6. Comparasion of various charaterization methods

Table S1 A summary of different methods for measuring the elasticity and adheison metrology of 2D materials.

Method	Sample fabrication	Equipment	Strength	Weakness	Ref.
Nanoindentation	Lithography;	AFM	Easy-to-use; Quick measurement of Young's modulus;	Subject to errors when decoupling pre-tension and Young's modulus terms	1-6
Nanomechanical resonator	Lithography; Metal deposition	Interferometer	Sensitive to pretension	Incapable of measuring adhesion	7-9
Tensile test	Lithography; Careful transfer	SEM	Direct fracture measurements	Incapable of measuring adhesion; Time consuming;	10-12
Spontaneous blister tests	Lithography; Metal deposition;	SEM or AFM or STM	Easy-to-use; Commonly observed;	Incapable of measuring elasticity;	13-18
Bulge test	Lithography;	AFM	Measuring Young's modulus and adhesion	Needs pressure control; Insensitive to pre-tension; Time-consuming;	19-22
Wrinkling	Elastomer	AFM	Easy-to-use; Commonly observed;	Incapable of measuring adhesion;	23
Pull-to-peel test	**Lithography; Metal deposition**	**SEM**	**Measuring Young's modulus and adhesion simultaneously**	**Sample damage; Insensitive to pre-tension;**	**Our work**

Here, we discuss mechanisms that lead to the defects on sample during the preparation process: 1. Thermal effect. 2. High energy metal atoms bombardment. 3. Deposition pressure. 4. Electron beam irradiation.[24, 25]

In some measurements where minimal defects are desirable, we suggestion refined sample preparation process as follows: 1. Reducing deposition rate. 2. Lowering the deposition temperature. 3. Reducing electron beam does.

7. Summary of experimental results.

Table S2. A summary of our measurements in the pull-to-peel test. Note that the size of the top flat end of the blister (i.e., the radius of the metal disk, a) is fixed to be 1.5 μm.

Sample	Condition	F (mN)	h (μm)	b (μm)	d (nm)	$K_h \geqslant 12h^2/t^2$	a/b
G1 (t = 85 ± 3 nm)	Blister generation	0.18 ± 0.02					
	Circular blister	0.17 ± 0.02	0.26 ± 0.02	5.8 ± 0.1		114.5	0.259 ± 0.004
	Circular blister	0.20 ± 0.02	0.34 ± 0.02	7.4 ± 0.1		189.2	0.202 ± 0.003
	Circular blister	0.21 ± 0.02	0.38 ± 0.02	7.8 ± 0.1		233.6	0.193 ± 0.002
	Blister fracture	0.24 ± 0.02	0.70 ± 0.02	~13.5 ± 0.1	8.5 ± 0.5	814.0	0.111 ± 0.001
G2 (t = 95 ± 3 nm)	Blister generation	0.17 ± 0.02					
	Circular blister	0.17 ± 0.02	0.14 ± 0.02	3.7 ± 0.1		26.2	0.40 ± 0.01
	Circular blister	0.16 ± 0.02	0.20 ± 0.02	4.9 ± 0.1		54.7	0.308 ± 0.006
	Circular blister	0.15 ± 0.02	0.15 ± 0.02	4.0 ± 0.1		29.8	0.38 ± 0.01
	Circular blister	0.14 ± 0.01	0.12 ± 0.02	3.4 ± 0.1		17.7	0.44 ± 0.01
	Blister fracture	0.15 ± 0.02	0.47 ± 0.02	~9.2 ± 0.1	6.0 ± 0.5	291.3	0.163 ± 0.002
G3 (t = 49 ± 2 nm)	Blister generation	0.15 ± 0.02					
	Circular blister	0.14 ± 0.02	0.10 ± 0.02	2.9 ± 0.1		55.9	0.52 ± 0.02
	Circular blister	0.19 ± 0.02	0.12 ± 0.02	3.0 ± 0.1		78.1	0.49 ± 0.02
	Circular blister	0.20 ± 0.02	0.17 ± 0.02	3.6 ± 0.1		141.5	0.41 ± 0.01
	Circular blister	0.19 ± 0.02	0.17 ± 0.02	3.7 ± 0.1		149.7	0.41 ± 0.01
	Circular blister	0.26 ± 0.03	0.20 ± 0.02	4.0 ± 0.1		203.8	0.38 ± 0.01
	Blister fracture	0.26 ± 0.03	0.23 ± 0.02	~4.0 ± 0.1	8.0 ± 0.5	260.7	0.37 ± 0.01
G4 (t = 1.1 ± 0.1 nm)	Blister generation	0.10 ± 0.01					
	Circular blister	0.08 ± 0.01	0.34 ± 0.02	3 ± 0.1		1146446.3	0.5 ± 0.02
	Circular blister	0.09 ± 0.01	0.48 ± 0.02	3.75 ± 0.1		2284958.7	0.4 ± 0.01
	Blister fracture	0.09 ± 0.01	0.48 ± 0.02	3.75 ± 0.1	1.1 ± 0.1	2284958.7	0.4 ± 0.01
M1 (t = 195 ± 5 nm)	Blister generation	0.25 ± 0.03					
	Circular blister	0.23 ± 0.02	0.28 ± 0.02	5.1 ± 0.1		24.8	0.294 ± 0.006
	Circular blister	0.24 ± 0.02	0.37 ± 0.02	6.4 ± 0.1		43.2	0.233 ± 0.004
	Circular blister	0.24 ± 0.02	0.46 ± 0.02	7.5 ± 0.1		66.7	0.199 ± 0.003
	SEMGLU fracture						
M2 (t = 81 ± 3 nm)	Blister generation	0.22 ± 0.02					
	Circular blister	0.28 ± 0.03	0.50 ± 0.02	6.2 ± 0.1		452.1	0.244 ± 0.004
	Circular blister	0.29 ± 0.03	0.52 ± 0.02	6.1 ± 0.1		489.8	0.246 ± 0.004
	Blister fracture	0.29 ± 0.03	0.53 ± 0.02	~6.1 ± 0.1	8.0 ± 0.5	509.2	0.248 ± 0.004
M3 (t = 25 ± 2 nm)	Blister generation	0.24 ± 0.03					
	Circular blister	0.20 ± 0.02	0.53 ± 0.02	4.8 ± 0.1		5327.6	0.313 ± 0.007
	Circular blister	0.21 ± 0.02	0.58 ± 0.02	5.3± 0.1		6390.7	0.286 ± 0.005
	Circular blister	0.22 ± 0.02	0.65 ± 0.02	5.8 ± 0.1		8166.6	0.260 ± 0.005
	Circular blister	0.24 ± 0.02	0.75 ± 0.02	6.3 ± 0.1		10872.7	0.237 ± 0.004
	SEMGLU fracture						

Section III: Theoretical model

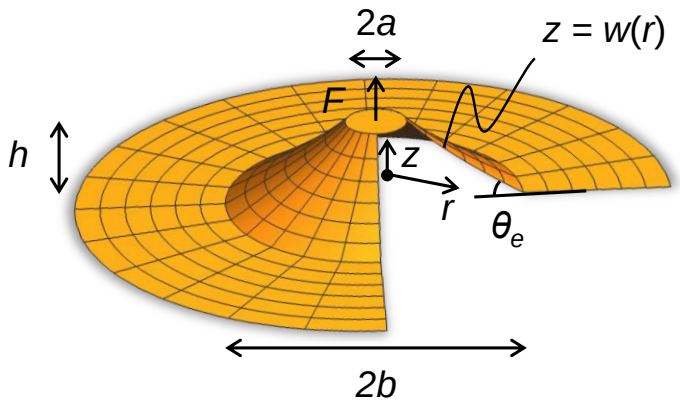

Fig. S6. Notations for the analysis of the blister mechanics.

In the main text we have specified the problem in the form of free energies of the systems:

$$\Pi = U_{\text{elastic}} + U_{\text{external}} - \pi b^2 \Gamma, \tag{S1}$$

where U_{elastic} is the stretching energy stored in the deformed nanoflake. Without loss, we focus on a displacement-controlled analysis so that external work vanishes. We assume a no-slip condition at the solid-solid interface so the elastic energy can be written in a way to only include the deflected part:

$$U_{\text{elastic}} = 2\pi \int_a^b \frac{1}{2}(N_r \epsilon_r + N_\theta \epsilon_\theta) r \mathrm{d}r\,, \tag{S2}$$

where N_r and N_θ are, respectively, the radial and hoop stress resultant, and ϵ_r and ϵ_θ are, respectively, the radial and hoop strain. We note that the slip between the nanoflake and the gold substrate appears not significant in "regular" blisters since we did not see clear evidence for the occurrence of wrinkling instabilities in the peeled, suspended part of the nanoflake, which has been thought of as the signature of slips in large FvK number systems. To obtain the governing equations for the mechanics of blisters, we perform a variational analysis, i.e.,

$$\delta\Pi = 0, \tag{S3}$$

with a no-pinning condition (so delamination is allowed)

$$\delta b \neq 0. \tag{S4}$$

The standard variational analysis can readily lead to the in-plane and out-of-plane equilibrium equations:

$$N_r \kappa_r + N_\theta \kappa_\theta = 0 \tag{S5}$$

and

$$\frac{\mathrm{d}N_r}{\mathrm{d}r} + \frac{N_r - N_\theta}{r} = 0, \tag{S6}$$

where κ_r and κ_θ are the radial and hoop curvature of the deformed nanoflake, respectively. Under the assumption of moderate rotation, we may write the curvatures as

$$\kappa_r = \frac{\mathrm{d}^2 w}{\mathrm{d}r^2} \quad \text{and} \quad \kappa_\theta = \frac{\mathrm{d}w}{r\mathrm{d}r}, \tag{S7}$$

where w is the deflection (Fig. S5). Four natural boundary conditions could be obtained in the variational analysis:

$$u(a) = u(b) = w(b) = 0 \quad \text{and} \quad w(a) = h, \tag{S8}$$

stating zero in-plane displacements u at $r = a$ and $r = b$ (because of no-slip), zero out-of-plane displacements at the blister edge, and an imposed blister height at the blister center, respectively.

It is much more convenient to use the Airy stress function Φ to rewrite the governing equations as[26, 27]

$$\Phi \frac{\mathrm{d}^2 w}{\mathrm{d}r^2} + \frac{\mathrm{d}\Phi}{\mathrm{d}r}\frac{\mathrm{d}w}{\mathrm{d}r} = 0 \tag{S9}$$

and

$$r\frac{\mathrm{d}}{\mathrm{d}r}\left[\frac{1}{r}\frac{\mathrm{d}}{\mathrm{d}r}(r\Phi)\right] + \frac{1}{2}\left(\frac{\mathrm{d}w}{\mathrm{d}r}\right)^2 = 0. \tag{S10}$$

Note that $N_r = \Phi/r$ and $N_\theta = \mathrm{d}\Phi/\mathrm{d}r$ so that Eq. (S6) is satisfied automatically; Eq. (S10) essentially comes from the requirement of compatibility.

One may have realized that the four boundary conditions are not enough to solve the two 2nd order ordinary differential equations specified in Eqs. (S9) and (S10) because the blister radius is unknown *a priori*. Indeed, as we have discussed in the main text, the blister radius is selected to minimize the potential energy and therefore is a result of the balance between elastic and adhesive forces. This condition could be given by considering the boundary terms associated with $\delta b \neq 0$, reading

$$N_e(1-\cos\theta_e) - \Gamma + \frac{1}{2}N_e\epsilon_e = 0, \tag{S11}$$

i.e., Eq. (7) in the main test. With Eqs. (S8-S11), we are able to solve this system numerically for example via ODE solver bvp5c in MATLAB. In Figs. S6 a nd S7, we verify the analytical models we presented in the main text, i.e., Eqs. (3) and (8), via numerical results as well as compare them with relevant models available in the literature.

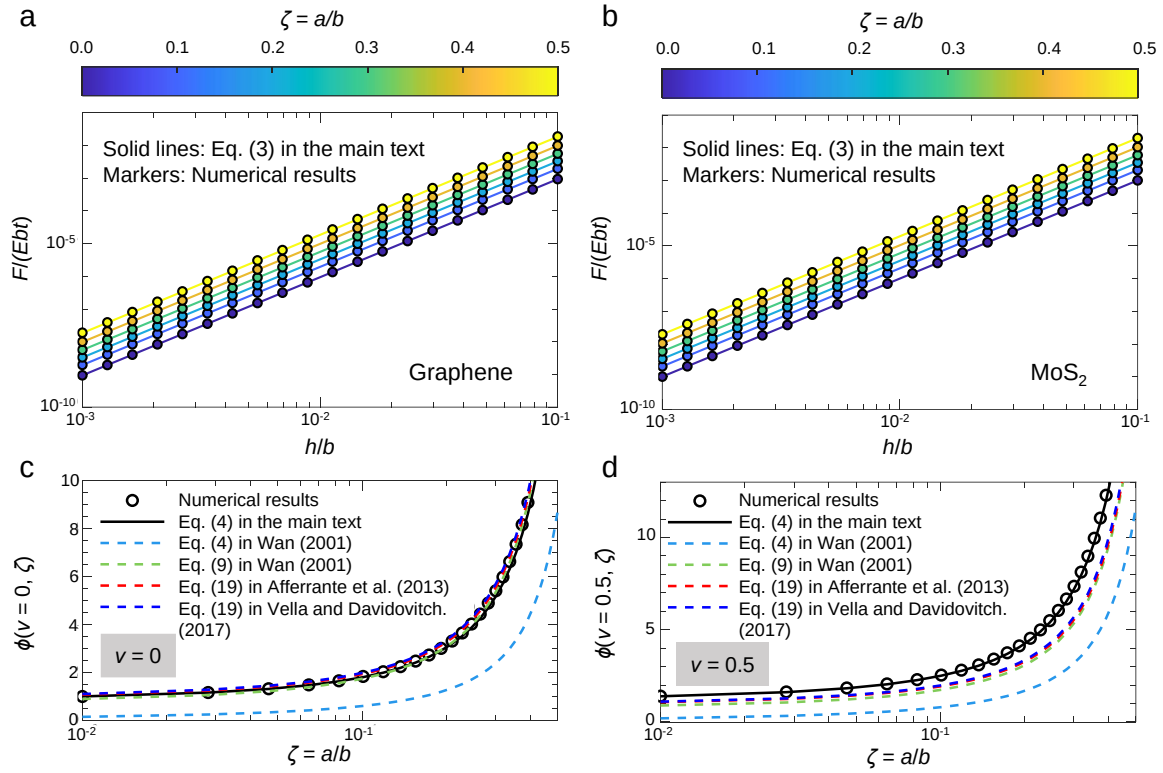

Fig. S7. Comparison between numerical results and various analytical models that can be used for Young's modulus measurements. a. Normalized pulling force as a function of the normalized blister height for graphene using $\nu = 0.165$. **b.** Normalized pulling force as a function of the aspect ratio of the blister for MoS_2 using $\nu = 0.27$. In **a** and **b**, the effect of the

finite size of the loading zone is presented by the value of $\zeta = a/b$. Markers are based on numerical calculations and solid curves are plotted based on Eq. (3) in the main test. The line and marker color are used to encode ζ as in the associated color bar. The prefactor for the force-height relation is numerically calculated for $\nu = 0$ (markers in **c**) and $\nu = 0.5$ (markers in **d**). The solid curves come from the model we used in the main text while dashed curves are from models in the literature (obtained by using various approximations)[28-30].

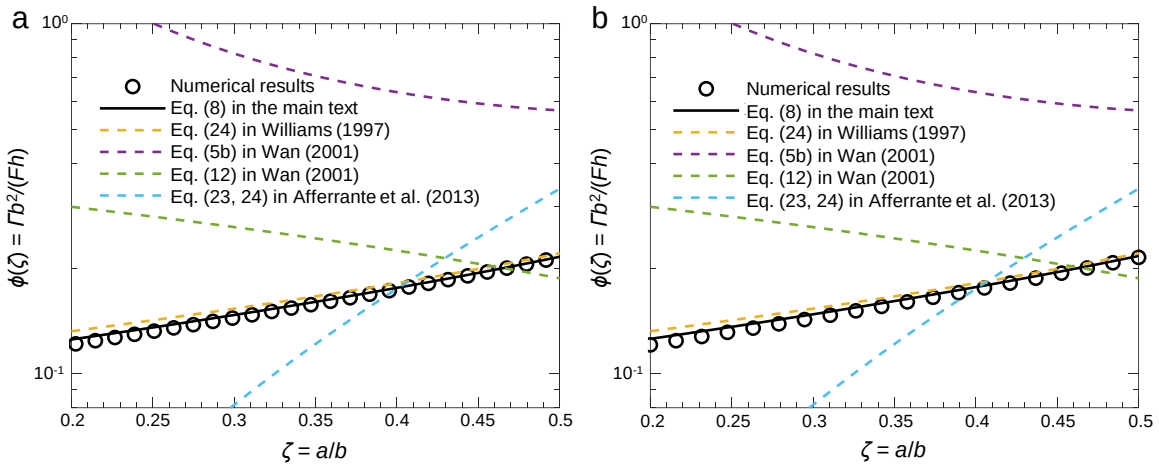

Fig. S8. Comparison between numerical results and various analytical models for adhesion measurements. a. Results for graphene using $\nu = 0.165$. **b.** Results for MoS_2 using $\nu = 0.27$. Markers are numerical calculations, solid curves are plotted based on Eq. (3) in the main test, and dashed curves are from relevant models in the literature[29-31].

1. Changgu, L.; Xiaoding, W.; Kysar, J. W.; James, H. Measurement of the elastic properties and intrinsic strength of monolayer graphene. *Science* **2008,** 321 (5887), 385-388.
2. Bertolazzi, S.; Brivio, J.; Kis, A. Stretching and Breaking of Ultrathin MoS2. *ACS Nano* **2011,** 5 (12), 9703-9709.
3. Castellanos-Gomez, A.; Poot, M.; Steele, G. A.; van der Zant, H. S. J.; Agraït, N.; Rubio-Bollinger, G. Elastic Properties of Freely Suspended MoS2 Nanosheets. *Adv. Mater.* **2012,** 24 (6), 772-775.
4. Falin, A.; Cai, Q.; Santos, E. J. G.; Scullion, D.; Qian, D.; Zhang, R.; Yang, Z.; Huang, S.; Watanabe, K.; Taniguchi, T.; Barnett, M. R.; Chen, Y.; Ruoff, R. S.; Li, L. H. Mechanical properties of atomically thin boron nitride and the role of interlayer interactions. *Nat. Commun.* **2017,** 8 (1), 15815.
5. Sun, Y.; Pan, J.; Zhang, Z.; Zhang, K.; Liang, J.; Wang, W.; Yuan, Z.; Hao, Y.; Wang, B.; Wang, J.; Wu, Y.; Zheng, J.; Jiao, L.; Zhou, S.; Liu, K.; Cheng, C.; Duan, W.; Xu, Y.; Yan, Q.; Liu, K. Elastic Properties and Fracture Behaviors of Biaxially Deformed, Polymorphic MoTe2. *Nano Lett.* **2019,** 19 (2), 761-769.
6. Liu, K.; Yan, Q.; Chen, M.; Fan, W.; Sun, Y.; Suh, J.; Fu, D.; Lee, S.; Zhou, J.; Tongay, S.; Ji, J.; Neaton, J. B.; Wu, J. Elastic Properties of Chemical-Vapor-Deposited Monolayer MoS2, WS2, and Their Bilayer Heterostructures. *Nano Lett.* **2014,** 14 (9), 5097-5103.
7. Lee, J.; Wang, Z.; He, K.; Shan, J.; Feng, P. X. L. High Frequency MoS2 Nanomechanical Resonators. *ACS Nano* **2013,** 7 (7), 6086-6091.
8. Wang, Z.; Jia, H.; Zheng, X.-Q.; Yang, R.; Ye, G. J.; Chen, X. H.; Feng, P. X. L. Resolving and Tuning Mechanical Anisotropy in Black Phosphorus via Nanomechanical Multimode Resonance Spectromicroscopy. *Nano Lett.* **2016,** 16 (9), 5394-5400.
9. Zheng, X.-Q.; Lee, J.; Feng, P. X. L. Hexagonal boron nitride nanomechanical resonators with spatially visualized motion. *Microsyst. Nanoeng.* **2017,** 3 (1), 17038.
10. Zhang, P.; Ma, L.; Fan, F.; Zeng, Z.; Peng, C.; Loya, P. E.; Liu, Z.; Gong, Y.; Zhang, J.; Zhang, X.; Ajayan, P. M.; Zhu, T.; Lou, J. Fracture toughness of graphene. *Nat. Commun.* **2014,** 5 (1), 3782.
11. Yang, Y.; Li, X.; Wen, M.; Hacopian, E.; Chen, W.; Gong, Y.; Zhang, J.; Li, B.; Zhou, W.; Ajayan, P. M.; Chen, Q.; Zhu, T.; Lou, J. Brittle Fracture of 2D MoSe2. *Adv. Mater.* **2017,** 29 (2), 1604201.
12. Yang, Y.; Song, Z.; Lu, G.; Zhang, Q.; Zhang, B.; Ni, B.; Wang, C.; Li, X.; Gu, L.; Xie, X.; Gao, H.; Lou, J. Intrinsic toughening and stable crack propagation in hexagonal boron nitride. *Nature* **2021,** 594 (7861), 57-61.
13. Zong, Z.; Chen, C.-L.; Dokmeci, M. R.; Wan, K.-t. Direct measurement of graphene adhesion on silicon surface by intercalation of nanoparticles. *J. Appl. Phys.* **2010,** 107 (2), 026104.
14. Gao, X.; Yu, X.; Li, B.; Fan, S.; Li, C. Measuring Graphene Adhesion on Silicon Substrate by Single and Dual Nanoparticle-Loaded Blister. *Adv. Mater. Interfaces* **2017,** 4 (9), 1601023.
15. Torres, J.; Zhu, Y.; Liu, P.; Lim, S. C.; Yun, M. Adhesion Energies of 2D Graphene and MoS2 to Silicon and Metal Substrates. *Phys. Status Solidi A* **2018,** 215 (1), 1700512.
16. Sanchez, D. A.; Dai, Z.; Wang, P.; Cantu-Chavez, A.; Brennan, C. J.; Huang, R.; Lu, N. Mechanics of spontaneously formed nanoblisters trapped by transferred 2D crystals. *Proc. Natl. Acad. Sci. U.S.A.* **2018,** 115 (31), 7884-7889.
17. Blundo, E.; Yildirim, T.; Pettinari, G.; Polimeni, A. Experimental Adhesion Energy in van der Waals Crystals and Heterostructures from Atomically Thin Bubbles. *Phys. Rev. Lett.* **2021,** 127 (4), 046101.
18. Wang, J.; Sorescu, D. C.; Jeon, S.; Belianinov, A.; Kalinin, S. V.; Baddorf, A. P.; Maksymovych, P. Atomic intercalation to measure adhesion of graphene on graphite. *Nat. Commun.* **2016,** 7 (1), 13263.

19. Lloyd, D.; Liu, X.; Boddeti, N.; Cantley, L.; Long, R.; Dunn, M. L.; Bunch, J. S. Adhesion, Stiffness, and Instability in Atomically Thin MoS2 Bubbles. *Nano Lett.* **2017,** 17 (9), 5329-5334.
20. Wang, G.; Dai, Z.; Wang, Y.; Tan, P.; Liu, L.; Xu, Z.; Wei, Y.; Huang, R.; Zhang, Z. Measuring Interlayer Shear Stress in Bilayer Graphene. *Phys. Rev. Lett.* **2017,** 119 (3), 036101.
21. Koenig, S. P.; Boddeti, N. G.; Dunn, M. L.; Bunch, J. S. Ultrastrong adhesion of graphene membranes. *Nat. Nanotechnol.* **2011,** 6 (9), 543-546.
22. Di Giorgio, C.; Blundo, E.; Pettinari, G.; Felici, M.; Polimeni, A.; Bobba, F. Exceptional Elasticity of Microscale Constrained MoS2 Domes. *ACS Appl. Mater. Interfaces* **2021,** 13 (40), 48228-48238.
23. Iguiñiz, N.; Frisenda, R.; Bratschitsch, R.; Castellanos-Gomez, A. Revisiting the Buckling Metrology Method to Determine the Young's Modulus of 2D Materials. *Adv. Mater.* **2019,** 31 (10), 1807150.
24. Kim, C.; Moon, I.; Lee, D.; Choi, M. S.; Ahmed, F.; Nam, S.; Cho, Y.; Shin, H.-J.; Park, S.; Yoo, W. J. Fermi Level Pinning at Electrical Metal Contacts of Monolayer Molybdenum Dichalcogenides. *ACS Nano* **2017,** 11 (2), 1588-1596.
25. Liu, Y.; Guo, J.; Zhu, E.; Liao, L.; Lee, S.-J.; Ding, M.; Shakir, I.; Gambin, V.; Huang, Y.; Duan, X. Approaching the Schottky–Mott limit in van der Waals metal–semiconductor junctions. *Nature* **2018,** 557 (7707), 696-700.
26. Chopin, J.; Vella, D.; Boudaoud, A. The liquid blister test. *Proc. Math. Phys. Eng. Sci.* **2008,** 464 (2099), 2887-2906.
27. Dai, Z.; Rao, Y.; Lu, N. Two-dimensional crystals on adhesive substrates subjected to uniform transverse pressure. *Int. J. Solids Struct.* **2022,** 257, 111829.
28. Vella, D.; Davidovitch, B. Indentation metrology of clamped, ultra-thin elastic sheets. *Soft Matter* **2017,** 13 (11), 2264-2278.
29. Wan, K.-T. Adherence of an axisymmetric flat punch on a thin flexible membrane. *J Adhes* **2001,** 75 (4), 369-380.
30. Afferrante, L.; Carbone, G.; Demelio, G.; Pugno, N. Adhesion of elastic thin films: double peeling of tapes versus axisymmetric peeling of membranes. *Tribol. Lett.* **2013,** 52 (3), 439-447.
31. Williams, J. Energy release rates for the peeling of flexible membranes and the analysis of blister tests. *Int. J. Fract.* **1997,** 87 (3), 265-288.